Journal of Thermal Science Vol.19, No.1 (2010) 26–33

DOI: 10.1007/s11630-010-0026-4 **Article ID: 1003-2169(2010)01-0026-08**

Experimental Investigation of Separation and Transition Processes on a High-Lift Low-Pressure Turbine Profile Under Steady and Unsteady Inflow at Low Reynolds Number

Satta F.[1], Simoni D.[1], Ubaldi M.[1], Zunino P.[1] and Bertini F.[2]

1. DIMSET - Università di Genova, Via Montallegro 1, I-16145 Genova, Italy
2. Avio R&D, V. I Maggio, 99 I-10040 Rivalta (TO) - Italy

The effects induced by the presence of incoming wakes on the boundary layer developing over a high-lift low-pressure turbine profile have been investigated in a linear cascade at mid-span. The tested Reynolds number is 70000, typical of the cruise operating condition. The results of the investigations performed under steady and unsteady inflow conditions are analyzed. The unsteady investigations have been performed at the reduced frequency of f^+=0.62, representative of the real engine operating condition.

Profile aerodynamic loadings as well as boundary layer velocity profiles have been measured to survey the separation and transition processes. Spectral analysis has been also performed to better understand the phenomena associated with the transition process under steady inflow.

For the unsteady case, a phase-locked ensemble averaging technique has been employed to reconstruct the time-resolved boundary layer velocity distributions from the hot-wire instantaneous signal output.

The ensemble-averaging technique allowed a detailed analysis of the effects induced by incoming wakes-boundary layer interaction in separation suppression. Time-resolved results are presented in terms of mean velocity and unresolved unsteadiness time-space plots.

Keywords: boundary layer separation, boundary layer transition, wake-boundary layer interaction, high-lift profile, low-pressure turbine

Introduction

Since the modern tendency in low-pressure turbine design leads towards increased aerodynamic loading per blade with the objective of reducing the engine weight and costs, the study of the phenomena associated with high-lift profiles assumes a continuously increasing importance.

Especially at low Reynolds numbers, the high diffusion to which the blade suction side is subjected may induce boundary layer laminar separation and consequently loss increase. The boundary layer transition process plays a fundamental role in the separation bubble behaviour, since it is responsible for the promotion of boundary layer reattachment. Mayle [1], Walker [2], and Hatman et al. [3] presented in depth analyses of transitional phenomena in gas turbine engines. Different prediction models for the estimation of the bubble extension have been proposed, but there is no complete model to describe the overall separated flow transition process.

Received: November 2009
Francesca SATTA, Daniele SIMONI: Philosophy Doctors
Marina UBALDI, Pietro ZUNINO: Professors

Nomenclature

C	blade chord
c_D	bar drag coefficient
c_p	pressure coefficient $= (p_{t1} - p)/(p_{t1} - p_2)$
C_x	axial chord
d	bar diameter
f	instability frequency
f_{bar}	bar passing frequency
f^+	reduced frequency $= f_{bar} C/u_{2is}$
g	cascade pitch
g_{bar}	bar pitch
K	wave number$=2\pi f/u_{infl}$
l	separated shear layer thickness
p	static pressure
p_t	total pressure
Re	Reynolds number based on the blade chord and on the isentropic exit velocity $= u_{2is} C/\nu$
S	power spectral density of the velocity fluctuations
u'_{rms}	root mean square of the velocity fluctuations
t	time
T	wake passing period
t^*	non-dimensional time $= t/T$
u	time-averaged velocity
U_{bar}	bar rotation velocity
$\bar{u}$	average velocity between the shear layer boundaries
u_{2is}	isentropic exit velocity
u_{ref}	trailing edge freestream velocity
x	cascade axial coordinate
y	normal to the wall direction
Y_p	bars total pressure loss coefficient $c_D d/(g_{bar}\cos\beta)$
Zw	Zweifel number $= 2(g/C_x)\cos^2\alpha_2(\tan\alpha_1 - \tan\alpha_2)$

Greek letters

α	blade metal angle
β	wake relative flow angle
δ_w	vorticity thickness $= \Delta u/(\partial u/\partial y)_{\max}$
Δu	velocity difference between the shear layer boundaries
ν	kinematic viscosity
ρ	density
Φ	flow coefficient $= u_x/U_{bar}$
ω^*	dimensionless frequency $= 1/4\,\delta_w(2\pi f)/\bar{u}$

Subscripts and brackets

1	cascade inlet
2	cascade outlet
infl	on the line of the inflection points in the velocity distributions
$\langle\rangle$	ensemble-averaged quantity

Numerical and experimental studies on separated flows [4-7] showed that a two-dimensional inviscid instability originates inside the separated shear layer via the Kelvin-Helmholtz mechanism. Vortical structures are shed by this instability process and induce fluctuations inside the flow which promote the boundary layer transition.

When upstream wakes are present, the boundary layer transition may be promoted also by rotor-stator aerodynamic interaction, with a consequent attenuation of the separation bubble extension. This phenomenon has been described in several studies focused on the propagation of upstream wakes through the downstream blade rows [e.g. 8-11]. These works pointed out that the transition process is highly influenced by the wakes shed from the upstream blades, which usually promote a prompter bubble reattachment.

Halstead et al. [8] provided a systematic analysis of the boundary layer development in axial compressors and turbines, under unsteady inflow conditions. The upstream wakes introduce periodic velocity and turbulence fluctuations during their travel through the passage [12]. The turbulent spots generated during the wake-boundary layer interaction propagate downstream, in a way similar to that of a turbulent spot occurring in a by-pass transition process [13]. These turbulence cores promote an earlier transition process, which is beneficial for reducing the extension of the separation bubble, when the laminar separation is present under steady inflow.

Detailed boundary layer analyses on high-lift turbine cascades have been recently carried out to investigate the transition and separation phenomena, as well as the associated loss production mechanisms [14-16].

Even though experimental correlations have been obtained by many authors in the early stage of the research, in order to develop general transition models, the physi-

cal understanding of the separated flow transition has still to be improved for both steady and unsteady inflow conditions.

The present work is part of an extensive joint research activity of Avio and University of Genova, involving numerical and experimental activities, aimed at extending the knowledge on the unsteady wake-boundary layer interaction for high-lift profiles.

The paper gives an experimental account of the transition process occurring under both steady and unsteady inflow conditions, for Re = 70000 (typical of cruise operating condition), in a large scale linear cascade of high-lift LP turbine profiles. The boundary layer development has been surveyed at midspan by means of hot-wire traverses carried out along the blade suction side, within the separation and transition regions. Under unsteady inflow, the phase-locked ensemble averaging technique, triggered by the upstream wake passage, has been employed to reconstruct the time-dependent boundary layer velocity and unresolved unsteadiness distributions from the unsteady hot-wire instantaneous signal output.

Experimental Apparatus

The investigations have been carried out in a three-blade large-scale linear turbine cascade (Fig. 1), installed in an open-loop wind tunnel. The facility is described in detail in [17].

The tested profiles are high-lift low-pressure turbine blades; their main parameters are summarized in Table 1.

The presence of upstream rotor blades has been simulated by means of a tangential wheel of radial rods that rotates in a plane parallel to the cascade leading-edges plane. The axial distance between the bars and the blade leading edges is set to 33% of the blade axial chord.

Fig. 1 Test section

Table 1 Cascade main geometrical parameters

Chord length	C = 180 mm
Pitch to chord ratio	g/C = 1.05
Inlet metal angle	α_1 = 51°
Outlet metal angle	α_2 = –69°
Zweifel number	Zw = 1.19

The flow coefficient (Φ = 0.675) for the unsteady inflow tests was chosen to be representative of real engine operating conditions. The bar pitch was set equal to the cascade pitch, which resulted in a reduced frequency f^+ = 0.62.

The bar diameter (d=3 mm, equal to the trailing edge thickness) was chosen so that the wakes shed from the bars produce the same losses as those generated by a typical upstream low-pressure turbine row. The total pressure loss coefficient for the bars (Y_p) was estimated to be 3.3% of the cascade inlet dynamic pressure.

The suction side boundary layer has been surveyed by means of eleven traverses normal to the blade surface. Each traverse is constituted by 36 points, with smaller spacing close to the wall. The location of the boundary layer traverses and their corresponding reference numbers are shown in Fig. 2, and summarized in Table 2. The profile sketched in Fig. 2 is only indicative.

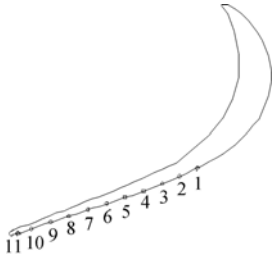

Fig. 2 Boundary layer measuring positions

Table 2 Traverses locations

Station	1	2	3	4	5	6	7	8	9	10	11
x/C_x	0.7	0.74	0.77	0.8	0.83	0.86	0.89	0.91	0.94	0.97	0.99

A Dantec single-sensor miniature boundary layer hot-wire probe (type 55P15) has been employed for the measurements. The hot-wire was operated in the constant temperature mode, using an overheat ratio of 0.8. Anemometer output voltages were sampled using a Metrabyte DAS 58 sample and hold AD converter board.

Time-mean measurements have been carried out collecting 140000 samples in each point with a sampling frequency of 40 kHz. An antialiasing low-pass filter set at 20 kHz has been used. The uncertainty in the velocity measurements has been evaluated to be lower than 2%, considering a confidence level of 95%.

Furthermore, the ensemble average technique has been employed to distinguish the periodic unsteadiness, associated with the bar passing frequency, from the velocity fluctuations associated with turbulence and unsteadiness not at the incoming wake frequency. Five contiguous rod passages have been investigated, collecting 188 data for

each rod passage, with a consequent record length of 940 data. In order to obtain a satisfactory statistical accuracy, 250 rotor revolutions have been acquired for ensemble averaging.

Results and discussion

Aerodynamic loadings

The profile aerodynamic loadings measured under steady and unsteady inflow conditions are compared in Fig. 3, where the static pressure distributions along the profile are plotted in terms of the static pressure coefficient, c_p.

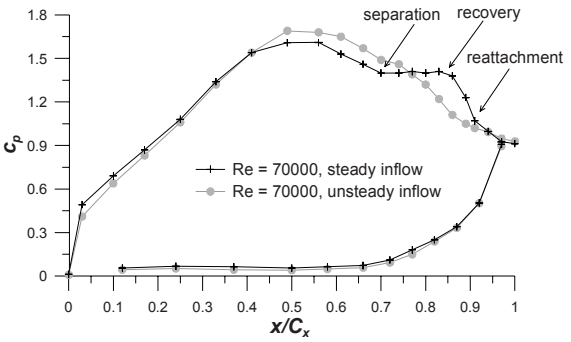

Fig. 3 Aerodynamic loadings under steady and unsteady inflow conditions

Under steady inflow condition, a large laminar separation bubble occurs on the profile suction side, as suggested by the long plateau present in the c_p distribution. Boundary layer separation occurs at x/C_x=0.70, whereas recovery and reattachment take place at around x/C_x=0.86 and x/C_x=0.91, respectively.

When incoming wakes are present, the length of the plateau on the suction side becomes evidently smaller, suggesting a drastic reduction of the separation bubble extension. That provokes an enhancement of the pressure coefficient peak, which generates a significant load increase as compared with the steady case.

Boundary layer mean velocity and unresolved unsteadiness distributions: steady inflow

The laminar separation bubble which affects the profile suction side under steady inflow was investigated by means of hot-wire measurements. In Fig. 4, the distributions of the time-mean velocity (normalized by the free-stream trailing edge velocity) measured in the bubble region are shown in a grey scale plot, with velocity vectors and the line of the inflection points in the velocity distributions superimposed.

This plot shows that boundary layer separation is already present at the first traverse investigated (x/C_x=0.70), consistently with the static pressure coefficient distribution that displays the beginning of a plateau just at this position. The separation bubble thickness grows getting downstream up to x/C_x = 0.86, where transition begins to occur, consistently with the recovery position identified by the c_p distribution.

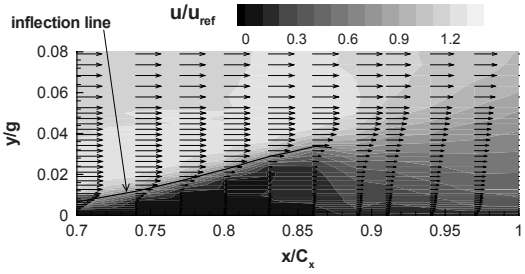

Fig. 4 Mean velocity grey scale plot under steady inflow condition

Downstream of this point, the bubble thickness decreases, and the low but not-null velocity near the wall indicates the beginning of reattachment, although the boundary layer may be intermittently separated and attached. In the proximity of x/C_x = 0.9, the mean velocity assumes higher values also in the region next to the wall, indicating that separation bubble reattachment has been completed. This is in agreement with the reattachment point identified in the profile aerodynamic loading.

In Fig. 5, mean velocity vectors have been superimposed to the unresolved unsteadiness grey scale plot to allow the identification of both stagnant fluid region and separated shear layer positions.

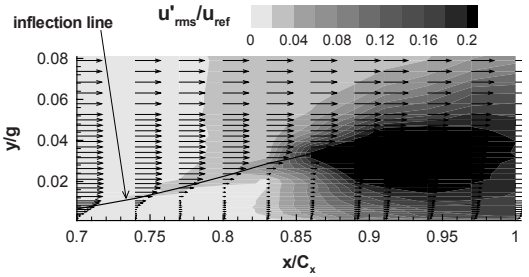

Fig. 5 Unresolved unsteadiness grey scale plot under steady inflow condition

Near zero values of the unresolved unsteadiness may be detected in the laminar part of the bubble (up to the recovery position, x/C_x=0.86), except for the larger values occurring above the stagnant fluid region, in correspondence of the line of inflection points in the velocity profiles, due to the shear layer instability. The large velocity fluctuations occurring inside the shear layer are due not only to the turbulence activity, but principally to the large scale structures that arise in the shear layer due to the inviscid instability process [18]. At x/C_x=0.86, the

unresolved unsteadiness in the shear layer starts to assume the highest values, due to the amplification of the coherent vortical structures shed by the bubble, and transition begins to occur in correspondence of the line of inflection points in the velocity profiles (x/C_x=0.86 and y/g=0.035). Successively, moving downstream, the high unresolved unsteadiness region propagates towards the wall, promoting the separation bubble reattachment.

The high fluctuations induced by the shear layer instability occur at a coherent frequency, which could be deduced from the spectra of velocity fluctuations obtained in correspondence of the line of inflection points in the velocity profiles.

In Fig. 6, the spectra evaluated at x/C_x = 0.83 and x/C_x = 0.86 in correspondence of the inflection line are compared. The presence of a peak around 180 Hz is clearly visible in both of the two distributions. These frequency peaks are associated with the vortex shedding phenomenon taking place in the separated shear layer. The magnitude increase of the frequency peak, which occurs when x/C_x increases, suggests that the instability process induces an amplification of the shear layer roll-up vortices. The peak frequency value displayed by the two spectra is in agreement with theoretical estimates of Kelvin-Helmholtz instability frequency range which is represented by the expression $0<Kl<1.2785$ [19], where K is the wave number and l is the separated shear layer thickness. For the present case, the product of the wave number and the separated shear layer thickness Kl has been evaluated to be equal to 0.938, hence included in the Kelvin-Helmholtz instability frequency range.

Morover, the dimensionless frequency of the instability process ω^* evaluated as suggested by Monkewitz and Huerre [20] has been found to be equal to 0.212. This value is in agreement with those found in other works reported in literature (e.g. [4-5, 21]) for different Reynolds number and adverse pressure gradient conditions.

Boundary layer ensemble averaged velocity and unresolved unsteadiness distributions: unsteady inflow

The boundary layer development when incoming wakes are present has been investigated by means of phase-locked measurements. The time-space plots of the ensemble averaged velocity and unresolved unsteadiness measured at several locations along the profile suction side are shown in Figs. 7-10.

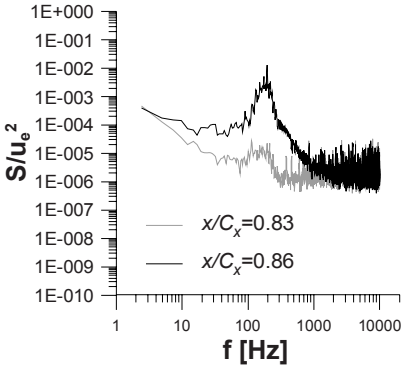

Fig. 6 Spectra of velocity fluctuations inside the shear layer at x/C_x=0.83 and x/C_x= 0.86

At x/C_x = 0.7, the mean velocity grey scale plot (Fig. 7, on the left side) shows the presence of a small stagnant fluid region at the wall in correspondence of t^*=0.4 and subsequent periods, consistently with the time-mean aerodynamic loading obtained under unsteady inflow condition, that displays the occurrence of separation onset just at this position. As shown by the unresolved unsteadiness grey scale plot (Fig. 7, on the right side), the incoming wake introduces inside the boundary layer a core characterized by high velocity fluctuations.

Moving downstream (x/C_x=0.77, Fig. 8), this high velocity fluctuations core grows both in magnitude and dimensions, and induces a localized boundary layer turbulent condition, which promotes separation bubble reattachment. In fact, at this position, during the turbulent spot (black areas in the right side plot of Fig. 8, the separation is suppressed, as displayed by the ensemble averaged velocity grey scale plot that shows an attached boundary layer for $0.5<t^*<0.7$. As soon as the effect induced by the incoming wake vanishes, boundary layer separation begins to occur again, and the bubble height grows when t^* increases, until the next incoming wake arrival.

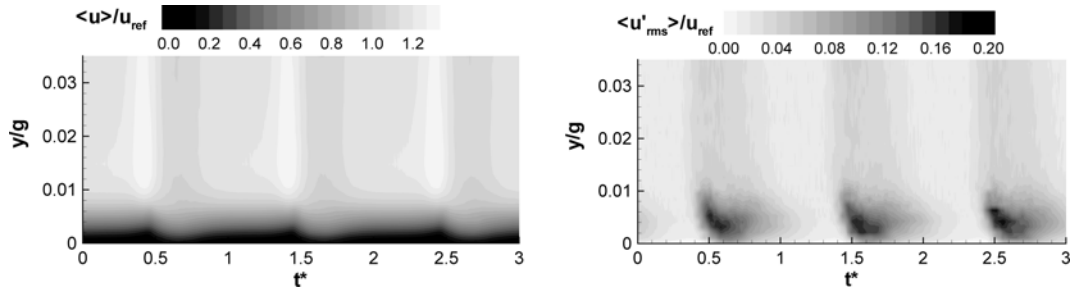

Fig. 7 Ensemble-averaged mean velocity and unresolved unsteadiness (x/C_x=0.7)

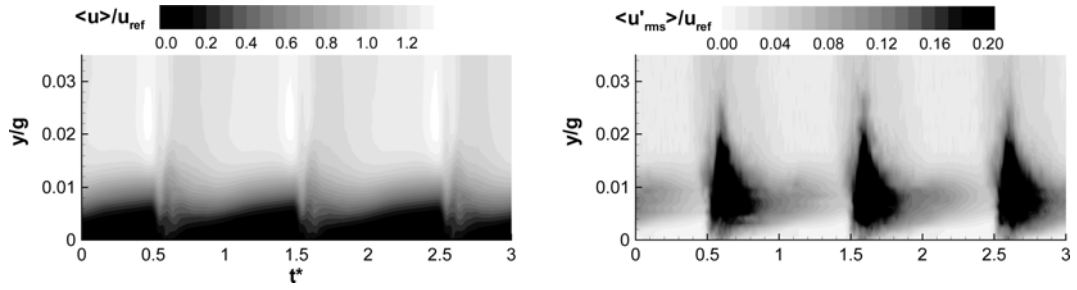

Fig. 8 Ensemble-averaged mean velocity and unresolved unsteadiness (x/C_x=0.77)

At x/C_x=0.83 (Fig. 9) the turbulent spot induced by incoming wake-boundary layer interaction is further on amplified. Moreover, a spontaneous transition process between two contiguous wakes, probably due to the same inviscid instability process detected under steady inflow, begins to occur inside the separated shear layer (the further high unresolved unsteadiness core centred in t^*=1.3, y/g=0.01). This core gives an additional contribution to the momentum transfer towards the wall. The larger extension of the high velocity fluctuations core associated with the incoming wake allows the suppression of the boundary layer laminar separation for a larger time interval compared with the upstream traverse (x/C_x=0.77). Furthermore, thanks to the natural instability process of the boundary layer between two contiguous wakes, the stagnant fluid region is further reduced around t^* =1.3.

To better understand the effects induced on the boundary layer by the two high velocity fluctuations cores, boundary layer phase-locked velocity and unresolved unsteadiness profiles measured at x/C_x=0.83 are reported in Fig. 11 for different t^* values.

At t^*=0.65 the incoming wake is already interacting with the suction side boundary layer, as shown by the large unresolved unsteadiness values measured in the free-stream. The turbulent core generated by the incoming wake-boundary layer interaction enhances the momentum transfer towards the wall, temporarily suppressing the separation, as shown by the shape of the phase-locked velocity profile, which presents not-null values also close to the wall for this time instant. When the effect of the incoming wake is almost completely vanished (t^*=1.15), the boundary layer laminar separation starts to take place again as suggested by the very small velocity values close to the wall. As soon as the boundary layer spontaneous transition, due to the instability process already discussed for the steady inflow case, takes place in the separated shear layer (t^*=1.35), a further enhancement of the momentum transfer towards the wall occurs and the phase-locked velocity close to the wall slightly increases. Successively, when the instability process is

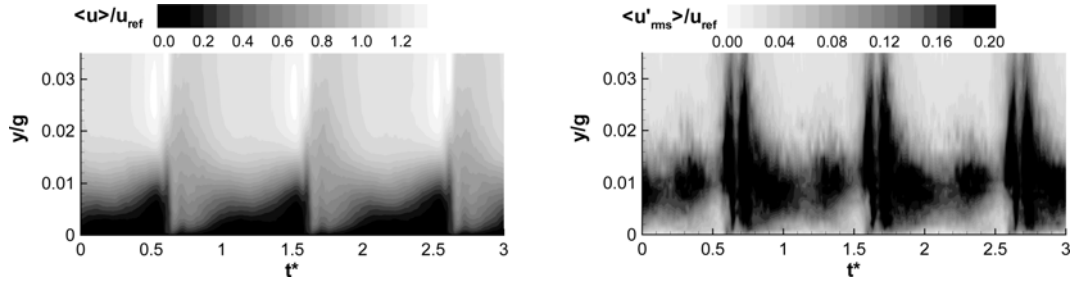

Fig. 9 Ensemble-averaged mean velocity and unresolved unsteadiness (x/C_x=0.83)

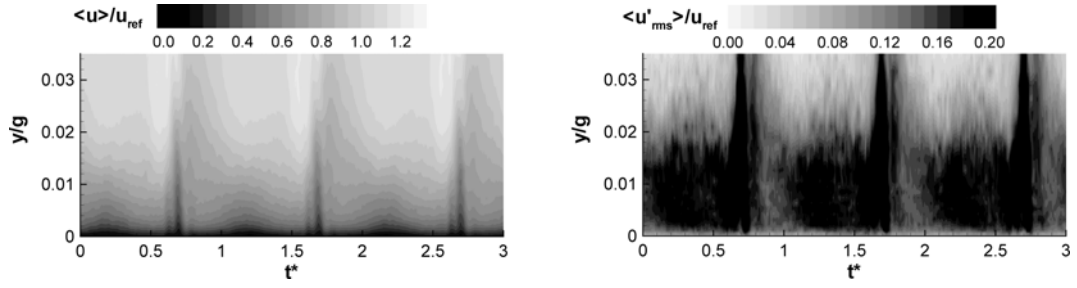

Fig. 10 Ensemble-averaged mean velocity and unresolved unsteadiness (x/C_x=0.86)

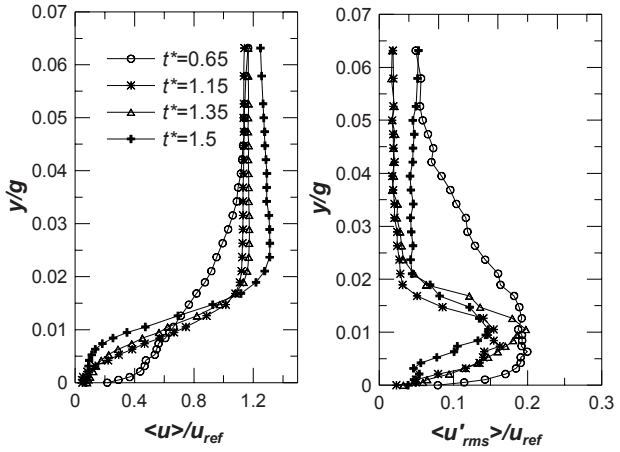

Fig. 11 Phase-locked velocity and unresolved unsteadiness at x/C_x=0.83 for different t^*

damped, the boundary layer laminar separation grows again and assumes its largest extension in correspondence of t^*=1.5, as observable by the phase-locked velocity profile.

Moving downstream from x/C_x=0.83, the two high unresolved unsteadiness cores (the one associated with the incoming wake-boundary layer interaction and that associated with the spontaneous transition between wakes) merge in a single high unresolved unsteadiness region which involves the whole wake passing period, inducing a fully turbulent boundary layer condition as shown by the grey scale plots at x/C_x=0.86 (Fig. 10). The momentum transfer associated with the turbulent condition allows the boundary layer reattachment, as demonstrated by the ensemble averaged velocity grey scale plot that shows not-null values also next to the wall at all the t^* values.

Conclusions

The transition and separation processes occurring along the suction side boundary layer of a high-lift low pressure turbine profile under both steady and unsteady inflow conditions have been investigated for a Reynolds number equal to 70000, representative of cruise condition.

Under steady inflow condition, the profile suction side has been found to be affected by a large laminar separation bubble. Aerodynamic loading distributions show that this bubble is strongly reduced when incoming wakes are present.

For the steady case, mean velocity and unresolved unsteadiness colour plots show that the beginning of boundary layer transition occurs in correspondence of the separated shear layer, along the line of inflection points in the velocity profiles, where the velocity fluctuations are larger due to the shear layer instability taking place through the Kelvin-Helmholtz mechanism. The velocity spectra show the peaks associated with the Kelvin-Helmholtz instability and demonstrate that fluctuations related to this instability process are amplified moving downstream along the line of inflection points in the velocity profiles. The fluctuations amplification is due to the shear layer rollup that continuously shed vortices, which grow in magnitude when the axial coordinate increases. As the fluctuations introduced in the boundary layer by the shear layer instability extend to the flow next to the wall, the increased mixing associated with the turbulent condition forces the boundary layer to reattach.

For unsteady inflow, transition and separation processes are shown to be strongly influenced by the incoming wakes and to become phase-dependent.

Time-space diagrams of the ensemble-averaged velocity and unresolved unsteadiness at different positions along the suction side display the large unresolved unsteadiness core associated with the incoming wake and its effect on the boundary layer development. This large velocity fluctuations core, which induces a localized boundary layer turbulent condition, and consequently separation bubble reattachment, has been found to be amplified getting downstream, where it covers a wider time interval. At x/C_x=0.83 another high velocity fluctuations core has been found to occur during the time interval between the wakes. It is associated with a spontaneous transition process between two contiguous wakes that begins to occur inside the separated shear layer (as it has been found to occur in the steady case) and is responsible for a further reduction of the stagnant fluid region.

When the two high unresolved unsteadiness cores (the one associated with the incoming wake-boundary layer interaction and another associated with the spontaneous transition between wakes) merge in a single high unresolved unsteadiness region for the whole wake passing period, a fully turbulent boundary layer condition is reached and the boundary layer reattachment is completed.

References

[1] Mayle, R. E.: The Role of Laminar-Turbulent Transition in Gas Turbine Engines, ASME J. Turbomach., Vol. 113, pp. 509–537, (1991).

[2] Walker, G. J.: The Role of Laminar-Turbulent Transition in Gas Turbine Engine: A Discussion, ASME J. Turbomachinery, Vol. 115, pp. 207–217, (1993).

[3] Hatman, A., and Wang, T.: A Prediction Model for Separated Flow Transition, ASME J. Turbomachinery, Vol. 121, pp. 594–602, (1999).

[4] Pauley, L. L., Moin, P., and Reynolds, W. C.: The Structure of Two-Dimensional Separation, J. Fluid Mech., Vol. 220, pp. 397–411, (1990).

[5] Yang, Z., and Voke, P. R.: Large-Eddy Simulation of Bounday-Layer Separation and Transition at a Change of Surface Curvature, J. Fluid Mech., Vol. 439, pp. 305–333, (2001).

[6] Malkiel, E., and Mayle, R. E.:Transition in a Separation Bubble, ASME J. Turbomach., Vol. 118, pp.752–759, (1996).

[7] Lou, W., and Hourmouziadis, J.: Separation Bubbles Under Steady and Periodic-Unsteady Main Flow Conditions, ASME J. Turbomach., Vol. 122, pp. 634–643, (2000).

[8] Halstead, D.E., Wisler, D.C., Okiishi, T,, Walker, G.J., Hodson, H.P. and Shin, H.W.: Boundary Layer Development in Axial Compressor and Turbines: Part 1 of 4 - Composite Picture, ASME Journal of Turbomachinery, Vol. 119, pp. 114–127, (1997).

[9] Mailach, R. and Vogeler, K.: Aerodynamic Blade Row Interaction in an Axial Compressor – Part I: Unsteady Boundary Layer Development, ASME Journal of Turbomachinery, Vol. 126, pp. 35–44, (2004).

[10] Schröder, Th.: Investigation of Blade Row Interaction and Boundary Layer Transition Phenomena in a Multistage Aero Engine Low-Pressure Turbine by Measurements with Hot-Film Probes and Surface-Mounted Hot-Film Gauges, in Boundary Layers in Turbomachines, VKI Lecture Series, Brussels (1991).

[11] Satta, F., Simoni, D., Ubaldi, M., Zunino, P., Bertini, F.: Boundary Layer Development on a High-Lift LP Turbine Profile under Passing Wakes Conditions, ASME Paper n°GT2009-59889, (2009).

[12] Stieger, R.D. and Hodson, H.P.: The Unsteady Development of a Turbulent Wake through a Downstream Low-Pressure Turbine Blade Passage, ASME Journal of Turbomachinery, Vol. 127, pp. 388–394, (2005).

[13] Jeon, W.P., Park, T.C. and Kang, S.H.: Experimental Study of Boundary-Layer Transition on an Airfoil Induced by Periodically Passing Wake, Experiments in Fluids, Vol. 32, pp. 229–241, (2002).

[14] Hodson, H.P. and Howell, R.J.: The Role of Transition in High-Lift Low-Pressure Turbines for Aeroengines, Progress in Aerospace Sciences, Vol. 41, pp. 419–454, (2005).

[15] Lazaro, B.J., Gonzalez, E. and Vazquez, R.: Temporal Structures of the Boundary Layer in Low Reynolds Number, Low Pressure Turbine Profiles, ASME Paper No. GT2008-50616, (2008).

[16] Schobeiri, M.T. and Pappu, K.: Experimental Study on the Effect of Unsteadiness on Boundary Layer Development on a Linear Turbine Cascade, Experiments in Fluids, Vol. 23, pp. 306–316, (1997).

[17] Satta, F., Simoni, D., Ubaldi, M., Zunino, P., Bertini, F. and Spano, E.: Time-Varying Flow at the Exit of a Highly Loaded LP Turbine Linear Cascade Under Unsteady Flow Conditions, Proceedings of the 8th European Turbomachinery Conference, Graz, (2009).

[18] Talan, M. and Hourmouziadis, J.: Characteristic Regimes of Transitional Separation Bubbles in Unsteady Flow, Flow Turbulence and Combustion, Vol. 69, pp. 207–227, (2002).

[19] Chandrasekhar, S.: Hydrodynamic and Hydromagnetic Stability, Oxford University Press, Oxford (1961).

[20] Monkewitz, P. A., and Huerre, P.:The Influence of the Velocity Ratio on the Spatial Instability of Mixing Layers, Phys. Fluids,Vol. 25, pp.1137–1143, (1982).

[21] Lengani, D., Simoni, D., Ubaldi, M., Zunino, P., Bertini, F.: An Experimental Study of the Reynolds Number Influence on a Laminar Separation Bubble, Ercoftac Bulletin, Vol. 80, (2009).